Int. J. Electrochem. Sci., 16 **(2021)** Article ID: 21053, doi: 10.20964/2021.05.01

International Journal of
ELECTROCHEMICAL
SCIENCE
www.electrochemsci.org

Combined First-principles and Experimental Studies of a V-doped $LiFePO_4$/C Composite as a Cathode Material for Lithium-ion Batteries

Qunfang Zhao[1,2,3], *Shuqiong Zhang*[1,2,3], *Chang Wang*[1,2,3], *Guanghui Jiang*[1,2,3], *Minyi Hu*[1,2,3], *Zhaoyong Chen*[4,*], *Quansheng Ouyang*[1,2,3,*]

[1] Advanced Batteries and Materials Engineering Research Center, Guizhou Light Industry Technical College, Guiyang 550025, China;
[2] Graphene Materials Engineering Research Center of Guizhou Colleges and Universities, Guiyang 550025, China;
[3] Provincial Collaborative Innovation Center of Used Power Batteries Recycling, Guiyang 550025, China;
[4] School of Materials Science and Engineering, Changsha University of Science and Technology, Changsha 410114, China;
[*]E-mail: qsouyang@163.com

Received: 4 November 2020 / *Accepted:* 11 Janary 2021 / *Published:* 31 March 2021

As a promising cathode material for lithium-ion batteries (LIBs), olivine-structured $LiFePO_4$ has been increasingly studied due to its high capacity, excellent thermal stability, cycling stability and environmental friendliness. Nevertheless, the main challenge of $LiFePO_4$ is its poor conductivity and Li^+ diffusion coefficient. Herein, a V-doped $LiFePO_4$/C composite is prepared via a solid-state method. The electronic structures of the samples are obtained by first-principles calculations based on density functional theory. V2 exhibits enhanced electrochemical performance, demonstrating discharge capacities as high as 155.6, 150.2, 136.0, 122.4 and 93.1 mA h g^{-1} at 0.1, 0.2, 0.5, 1.0 and 3.0C, respectively, and approximately 100% capacity retention after 100 cycles at 1.0C.

Keywords: Lithium-ion battery, $LiFePO_4$/C, First-principles, V-doped

1. INTRODUCTION

Under the background of an energy crisis and increasing environmental pollution, the development of lithium-ion batteries (LIBs) are of great interest as an ideal energy source in the 21st century due to their long cycling life, high power density and notable safety [1-4]. Olivine-structured $LiFePO_4$ has been considered one of the most competitive cathode materials for LIBs owing to its high theoretical capacity of 170 mA h g^{-1}, excellent thermal stability, cycling stability and environmental friendliness [5]. However, the poor conductivity and Li^+ diffusion coefficient of the above material limits its use in high-power applications. Enormous efforts have been devoted to enhancing conductivity, such as preparing nanoscale materials, coating with conductive carbon and doping other elements into the crystal lattice [6-12]. Nevertheless, it has been found that both increasing the content of a carbon coating and decreasing the particle size will result in a decreased tap density of the material [13]. Furthermore, the addition of electrochemically inert materials will lead to $LiFePO_4$ having a low energy density. Doping, first proposed by CHUNG et al. [14-17], has been proven to be able to enhance the electrical conductivity of $LiFePO_4$ by approximately 8 orders of magnitude. Thus, it has been considered one of the most effective methods to improve the conductivity of $LiFePO_4$ and has attracted the attention of many researchers. Liu et al. [18] reported that doping with Ni would improve the electrochemical performance of $LiFePO_4$. This research demonstrated that doped Ni enhanced the electrical conductivity of the material, resulting in a high capacity retention ratio of 93.9% after 200 cycles at 10C. At the same time, the electronic structures of pure and doped $LiFePO_4$ have been investigated by first-principles calculations [19-21].

Recent studies [22-24] have shown that proper V doping is beneficial for improving the electrochemical performance of $LiFePO_4$ cathode materials, especially the rate performance and cycling performance. Additionally, V_2O_5 has become a research focus as an electrochemically active compound. Chiang et al. [25] described that V substitutes at the lithium site in $LiFePO_4$, as shown by X-ray powder diffraction and neutron powder diffraction characterization, as well as increasing the volume of the unit cell since V acts as a nucleating agent to promote crystal growth. Presently, V occupying Fe sites in $LiFePO_4$ has been confirmed [26-28], and the volume of the unit cell is slightly larger on account of the change in lattice parameters. To date, the true roles of V-doped $LiFePO_4$ remain unclear and controversial. More importantly, little research has been reported on V-doped $LiFePO_4$ with theoretical calculations. Therefore, in this work, V-doped $LiFePO_4$/C samples are synthesized successfully via the solid-state method, and the electronic structures of all samples are calculated by first-principles calculations that are based on density functional theory. The effects of V doping on the crystal structures, electronic structures and electrochemical performance of $LiFePO_4$/C are explored through experimental studies combined with theoretical calculations.

2. EXPERIMENTAL

2.1. Computational method

Total energy and electronic structure calculations were explored through the use of the first-principles plane-wave pseudopotential method using the Cambridge serial total energy package (CASTEP) program in Materials Studio. A supercell was utilized for calculation. The traditional generalized gradient approximation (GGA) was limited to precisely compute the electronic structures of transition metal materials, ignoring the Coulomb repulsion between electrons. Hence, all calculations were carried out with the GGA+U and ultrasoft pseudopotential methods. Plane waves with a cutoff energy of 340 eV and a 3×4×5 k-point were used to ensure convergence of the total energy of the ground state and corresponded to an energy of 1.0×10^{-5} eV atom^{-1}.

2.2. Material preparation and characterization

$LiFe_{1-x}V_xPO_4/C$ (x=0, 0.01, 0.02, 0.03) samples were prepared by the solid-state method. To obtain the precursor, stoichiometric amounts of Li_2CO_3 (99.5%), $FeC_2O_4\cdot2H_2O$ (99.7%), $(NH_4)H_2PO_4$ (99.25%), and V_2O_5 were mixed with glucose by ball milling for 4 h in ethanol. Then, the sample was dried at 35 °C for 24 h to evaporate the ethanol. The dried mixture was ball-milled again for 30 min. Eventually, the $LiFe_{1-x}V_xPO_4/C$ (x=0, 0.01, 0.02, 0.03) cathode materials (V0, V1, V2, V3) with 3 wt.% carbon were formed by calcining at 400 °C for 6 h and then 750 °C for 15 h in N_2.

The crystal structures of all samples were observed via X-ray diffraction (XRD, Rigaku D/Max 200PC, Japan) with a graphite monochromator and a Cu Kα radiation source (λ=0.154505 nm). The morphology and elemental mapping results were obtained for V0 and V2 by scanning electron microscopy (SEM) and energy dispersive spectroscopy (EDS; OXFORD 7426, 20 kV)).

2.3. Electrochemical measurements

A CR2025 coin-type cell was used for electrochemical measurements. The as-prepared composites, acetylene black and polyvinylidene fluoride, were mixed at a weight ratio of 80:10:10, and the resulting slurry was coated on an Al-metal foil collector. A Celgard 2400 separator was used. The CR2025 coin-type cells (with V0, V1, V2 and V3 loadings of 4.00 mg·cm^{-2}) were assembled with a lithium-metal foil as the counter electrode in an argon-filled glovebox. The electrolyte was $LiPF_6$ (1.0 M)/ethylene carbonate + dimethyl carbonate (in a 1:1 volume ratio). Constant current-constant voltage (CC-CV) charge and galvanostatic discharge experiments were conducted over a voltage range of 2.5 to 4.1 V on a Land system (BT2001A). The electrochemical impedance spectroscopy (EIS) characterization of the composites was carried out in the frequency range of 10 mHz - 10^5 Hz using a CHI660B electrochemical workstation (Chenhua, Shanghai, China), with the perturbation amplitude controlled at ±5 mV.

3. RESULTS AND DISCUSSION

Table 1. Lattice parameters of V0, V1, V2 and V3 based on their XRD patterns

Sample	a [Å]	b [Å]	c [Å]	Cell volume [Å]^3
V0	10.3208	6.0046	4.6854	290.37
V1	10.3527	6.0099	4.6965	292.21
V2	10.3594	6.0085	4.7003	292.57
V3	10.3417	6.0161	4.6955	292.14

As shown in Fig. 1, the XRD patterns of the V0, V1, V2 and V3 composites can be indexed to olivine $LiFePO_4$ with an orthorhombic crystal structure and the Pama space group (JCPDS No. 81-1173); additionally, there are no impurity peaks after comparing to the V0 sample. Furthermore, no new phases exist, showing that a small amount of doped V will not change the crystal structure of $LiFePO_4$.

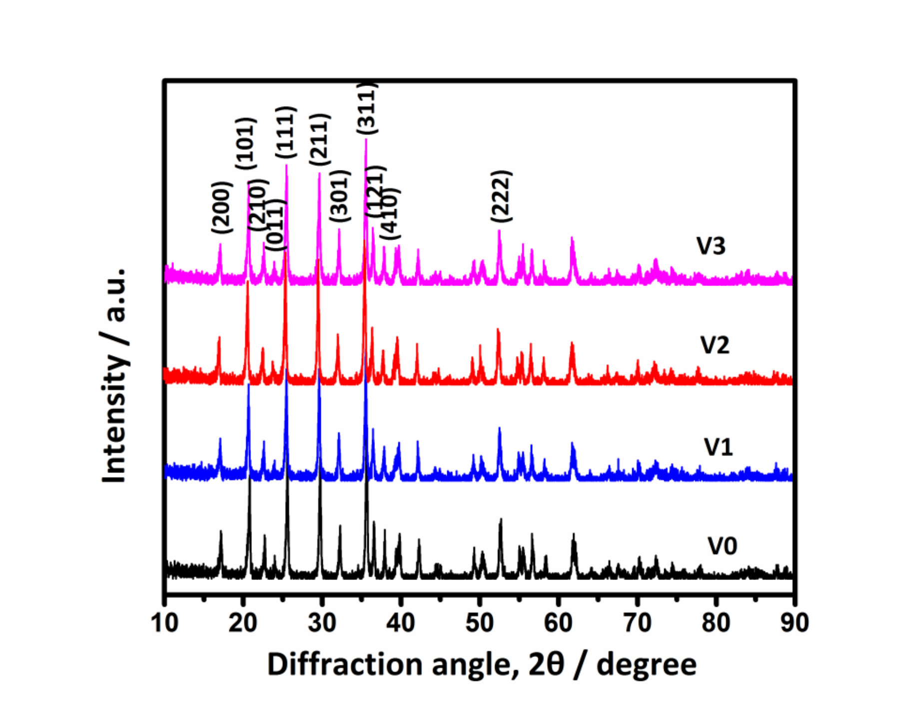

Figure 1. XRD patterns of V0, V1, V2 and V3

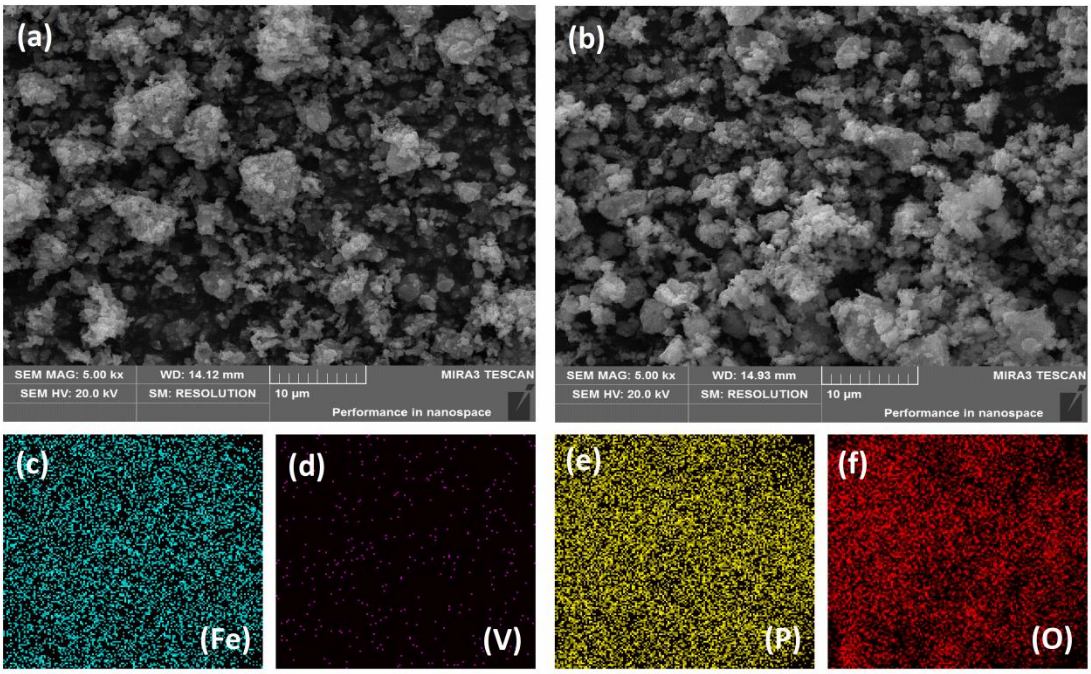

Figure 2. SEM images of (a) V0, (b) V2 and (c-f) the elemental mapping of V2 based on (b)

The lattice parameters of all samples, based on their XRD patterns, are presented in Table 1. Both the lattice parameters and volumes of all V-doped samples increase because the added V acts as a nucleating agent to promote crystal growth, which is consistent with a previous report [25]. As presented in Table 1, V2 has the largest a, c and V parameters, which expands the Li^+ diffusion path. Additionally, its small b parameter shortens the diffusion length of Li^+, which is better for the intercalation and deintercalation of Li^+.

As seen in the SEM images (Fig. 2a and 2b), V doping does not change the particle morphology and even makes the particles distribute more uniformly. Furthermore, V can be detected according to the EDS mapping results (Fig. 2d). Therefore, combined with the above XRD analysis, V is successfully doped into the $LiFePO_4$ crystal structure.

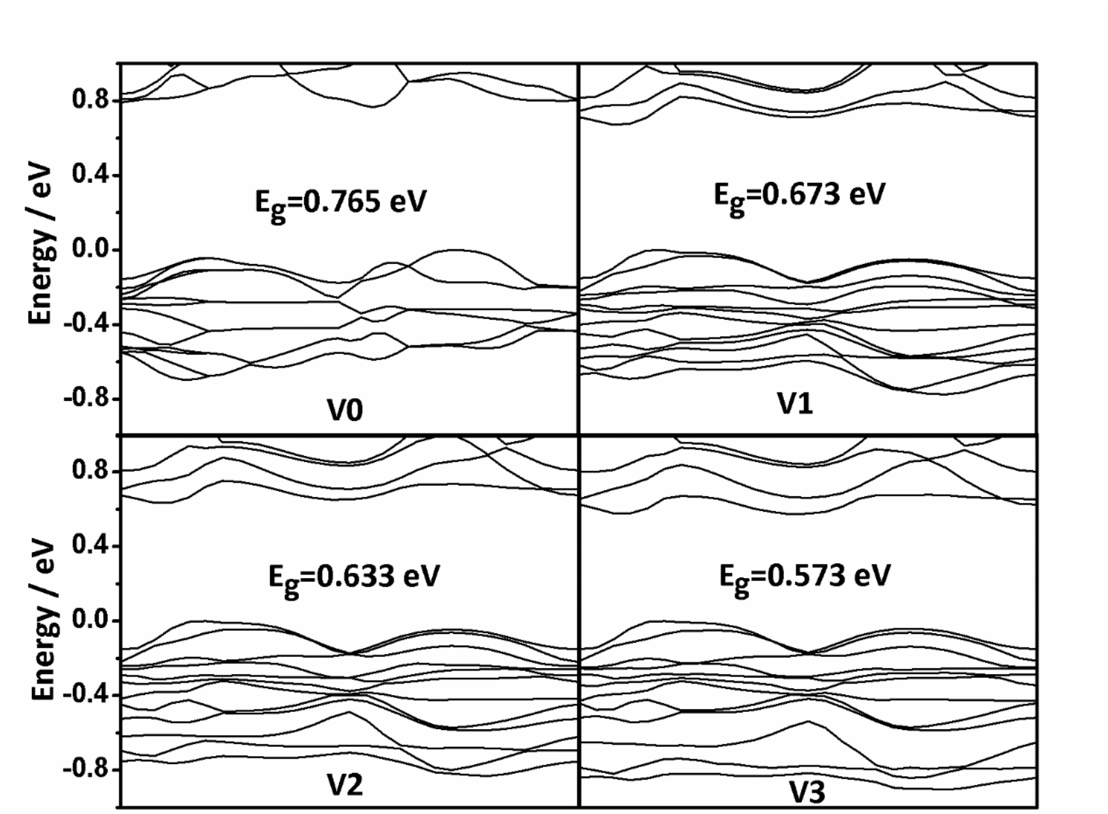

Figure 3. Band structures of the V0, V1, V2 and V3 samples as provided by first-principles calculations

To investigate the effects of V doping on the electronic structure and conductivity of $LiFePO_4$ cathode materials, we conducted first-principles calculations for the band structures of the V0, V1, V2 and V3 samples with the GGA+U method. As shown from the band structures (Fig. 3), the computational bandgaps (E_g) of V0, V1, V2 and V3 are 0.765, 0.673, 0.633 and 0.573 eV, respectively. Moreover, E_g decreases with an increasing amount of doped V, showing that V doping decreases the bandgap of $LiFePO_4$. A narrow bandgap can effectively reduce the transfer barrier of electrons, thereby leading to a material with higher electrical conductivity. However, V3 with a low E_g shows poor electrochemical properties. This result demonstrates that other factors also affect the electrochemical properties, such as the charge transfer impedance, which will be discussed later in this paper.

The effects of doping on the electronic structures of $LiFePO_4$ have attracted extensive attention by theoretical calculations. The electronic structures of pure and doped $LiFePO_4$ are evaluated via comparison with present first-principles investigations results based on DFT within the GGA or GGA+U level. Furthermore, the calculated bandgaps are listed in Table 2. The bandgaps of pure $LiFePO_4$ with 0.74 and 1.38 eV were acquired [29-30]. Xu's group [31] used first-principles calculations for exploring the electronic structure of doped $LiFePO_4$ at cation and anion sites. It has been found that doping caused narrower bandgaps (0.58, 0.39 and 0.05 eV for $Na_{1/8}Li_{1-1/8}FePO_4$, $LiMn_{1/8}Fe_{1-1/8}PO_4$ and $LiFePO_{4-1/32}F_{1/32}$, respectively). Similarly, the smaller bandgaps were obtained for N-doped $LiFePO_4$ (0.65 eV) [32] and $LiFe_{1-1/8}Mo_{1/8}PO_4$ (0.13 eV) [21]. Interestingly, the different calculation methods and parameter sets result in pure $LiFePO_4$ having various bandgaps. More importantly, it is rational to pay attention to the relative values. Compared with pure $LiFePO_4$, the bandgap is diminished by doping. Consequently, an appropriate doping is an effective method to improve the conductivity of $LiFePO_4$ materials.

Table 2. This work compared with other $LiFePO_4$ materials studied by first-principles calculations

	GGA (Eg, eV)	GGA+U (Eg, eV)	Reference
$LiFePO_4$	0.74		[29]
$LiFePO_4$		1.38	[30]
$Na_{1/8}Li_{1-1/8}FePO_4$	0.58		[31]
$LiMn_{1/8}Fe_{1-1/8}PO_4$	0.39		[31]
$LiFePO_{4-1/32}F_{1/32}$	0.05		[31]
N-$LiFePO_4$		0.65	[32]
$LiFe_{1-1/8}Mo_{1/8}PO_4$	0.13		[21]
V2		0.633	ours

The spin-polarized total density of states (DOS) and partial density of states (PDOS) of V0 (Fig. 4a) and V2 (Fig. 4b) were calculated with the GGA+U method to investigate the origin and relationship between the bandgaps and constituent elements. It is clear that the valence maximum and conduction band minimum are mainly contributed by the 3d electron of Fe in the lattice for V0. While it is mainly contributed by the 3d electrons of Fe and V for V2; furthermore, the PDOS of Li, P, and O shows almost no changes. Therefore, V doping decreases the bandgap of $LiFePO_4$.

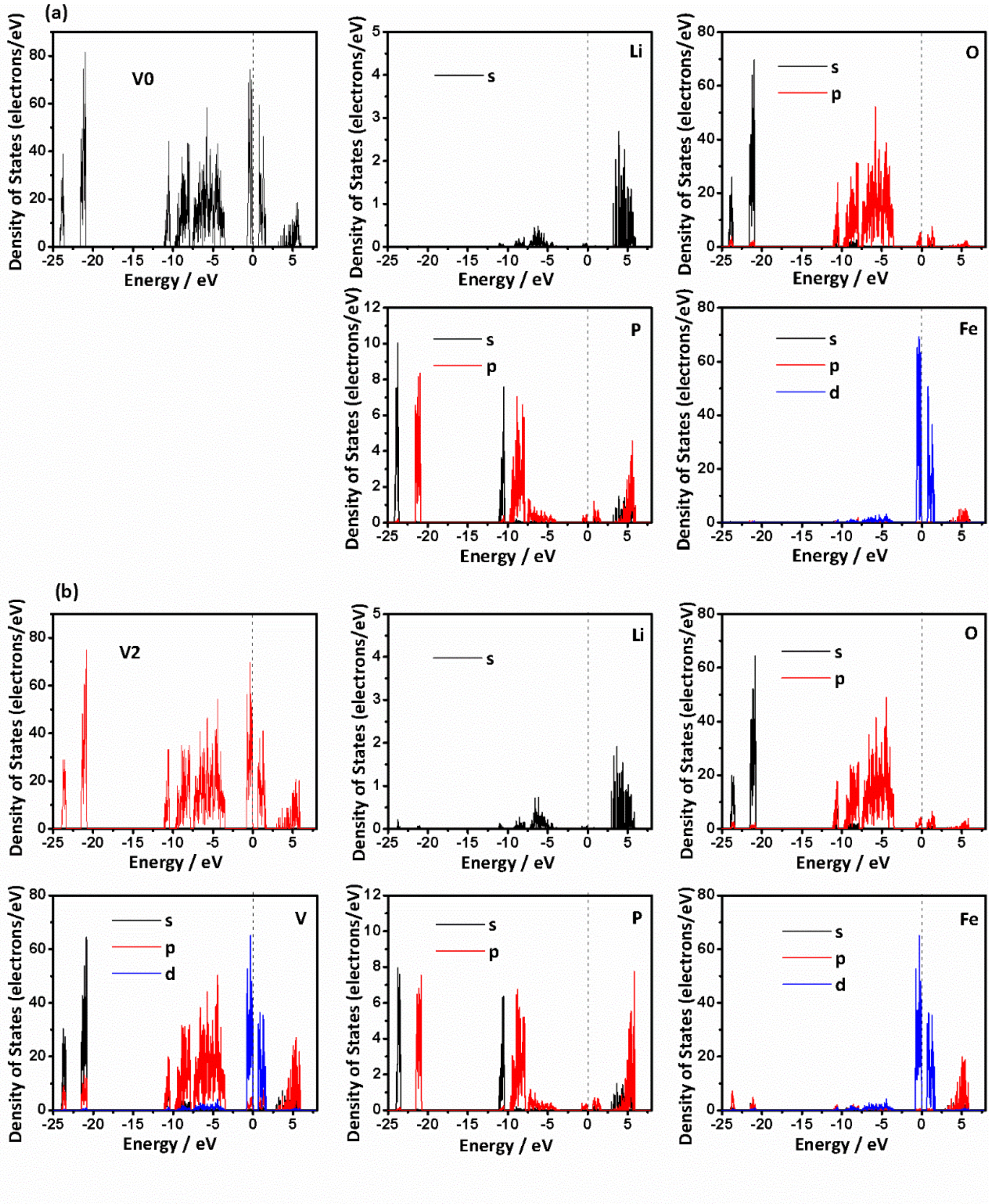

Figure 4. Total density of states (DOS) and partial density of states (PDOS) for (a) V0 and (b) V2

The galvanostatic charge and discharge tests of V0, V1, V2 and V3 were performed at 0.1C in a voltage range of 2.5-4.1 V at room temperature. As shown in Fig. 5a, the initial charge and discharge voltage profiles show a voltage plateau at 3.45 V for all samples, which corresponds to initial discharge capacities of 153.2, 146.8, 155.6 and 135.8 mA h g^{-1} for V0, V1, V2 and V3, respectively. The sample delivers the highest capacity of 155.6 mA h g^{-1} with a 2 wt% amount of doped V. Therefore, the most appropriate content of doped V is 2 wt%. To improve the electrochemical performance of $LiFePO_4$, vanadium modification has become one of the research hotspots. The V_2O_5 and NH_4VO_3 are frequently used as dopants to enhance electrochemical capacity and cyclic stability [33-39], as shown in Table 3.

Xu's group [34] confirmed the optimized sample by V_2O_5 doping delivered high discharge capacity of 154.3 mA h g^{-1} at 0.1C rate and capacity retention of approximately 100% at 1C rate. Chen's group [37] found that vanadium was entered into $LiFePO_4$ lattice to replace Fe^{2+} and improved electronic conductivity, giving rise to superior rate capability. In summary, the vanadium is doped at the Fe site, the above results are consistent with this theoretical and experimental results. Nevertheless, compared with other V-doped $LiFePO_4$ in Table3, V2 displays higher discharge capacity at 0.1C. As a consequence, the appropriate reaction conditions for V-doped $LiFePO_4$ benefit to excellent electrochemical properties.

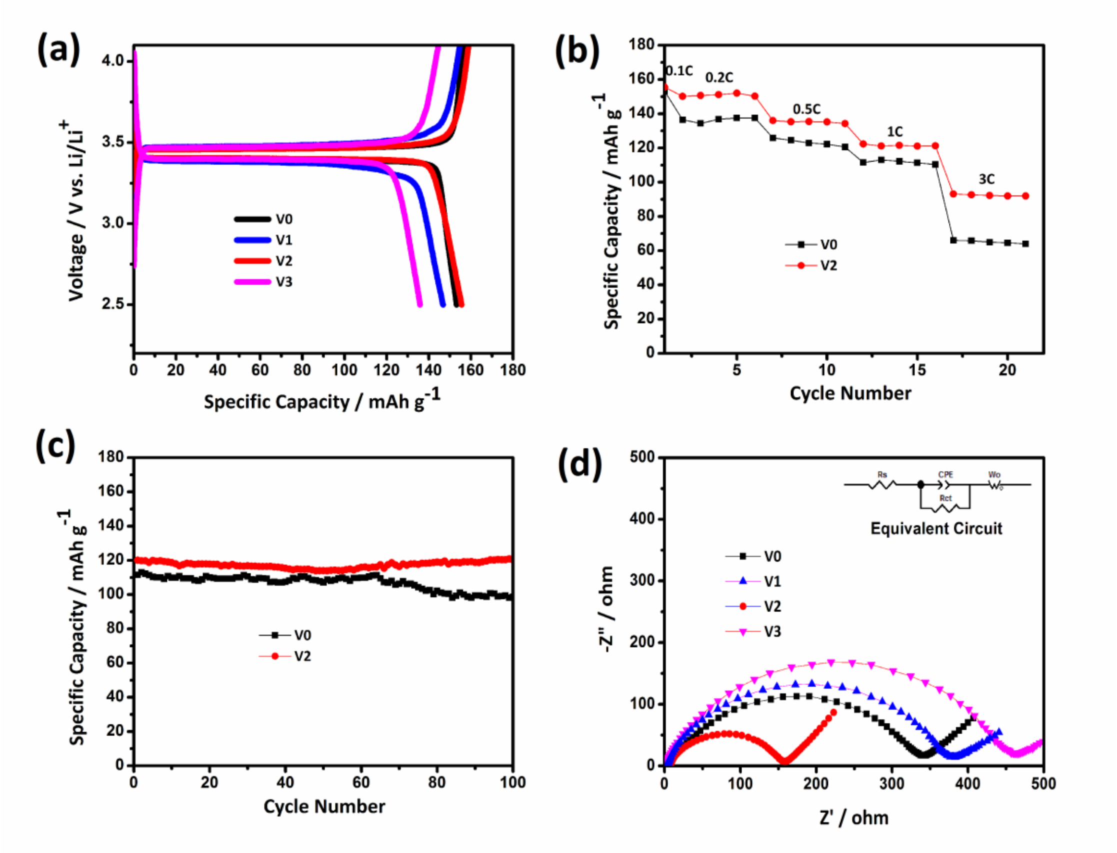

Figure 5. (a) Initial charge and discharge voltage profiles of V0, V1, V2 and V3 at a rate of 0.1C; (b) rate capabilities of V0 and V2 at rates from 0.1 to 3C; (c) cycling performance of V0 and V2 at 1C for 100 cycles; and (d) EIS of V0, V1, V2 and V3

Table 3. This work compared with other V-doped $LiFePO_4$ materials

	Dopant	Discharge capacity at 0.1 C rate	Reference
V2	V_2O_5	155.6 mA h g^{-1}	ours
$LiFe_{0.98}V_{0.02}PO_4$	V_2O_5	138 mA h g^{-1}	[33]
V^{5+} doping $LiFePO_4$	V_2O_5	154.3 mA h g^{-1}	[34]

$LiFe_{0.96}V_{0.04}PO_4$	NH_4VO_3	146.5 mA h g^{-1}	[35]
$LiFe_{0.96}V_{0.04}PO_4$	NH_4VO_3	141.1 mA h g^{-1}	[36]
$LiFe_{0.97}V_{0.03}PO_4$	NH_4VO_3	150.4 mA h g^{-1}	[37]
$LiFe_{0.97}V_{0.03}PO_4$	NH_4VO_3	151.4 mA h g^{-1}	[38]
$Li_{0.97}Fe_{0.93}V_{0.07}PO_4$	NH_4VO_3	153.5 mA h g^{-1}	[39]

Fig. 5b shows the discharge capacities of V0 and V2 on the grounds of various rates from 0.1 to 3.0C in the potential range of 2.5-4.1 V. It is clearly observed that the rate capability of V2 is superior to that of V0, especially at high rates. At a high rate of 3.0C, the reversible capacity of V2 can still reach 93.1 mA h g^{-1}, while V0 obtains only 66.0 mA h g^{-1}. This superior rate capability is attributed to the excellent electrical conductivity and improved Li^+ diffusion due to the doped V.

The cycling performances of V0 and V2 are evaluated at a 1C rate between 2.5 and 4.1 V. As shown in Fig. 5c, the initial discharge capacities of V0 and V2 at 1C are 111.5 and 120.1 mA h g^{-1}, respectively. Nevertheless, the discharge capacity of V0 is only 98.7 mA h g^{-1} (11.1% capacity loss) after 100 cycles. The capacity retention of V2 is approximately 100% after 100 cycles, which demonstrates that the proper content of doped V improves the cycling stability of the materials.

To compare the electrode kinetics of V0 and V2, we conducted electrochemical impedance spectroscopy (EIS) (Fig. 5d). The charge transfer resistance (R_{ct}) is applied to the electrolyte/active particle interface. The slope at the low frequency is attributed to Li^+ diffusion in the $LiFePO_4$/C particles, which indicates the Warburg impedance (Z_w). A simplified equivalent circuit model is established to study the impedance spectra, and the R_{ct} values of V0, V1, V2 and V3 are 337.5, 365.1, 155.2 and 446.4 Ω, respectively. The low R_{ct} indicates the high electrochemical activity and improved electrode kinetics of V2; thus, V2 has better electrochemical performance.

4. CONCLUSIONS

In summary, the V0, V1, V2 and V3 samples were successfully synthesized by the solid-state method, and the electronic structures of all samples were obtained by first-principles calculations based on density functional theory. V doping improves the electrical conductivity and electrode kinetics of the materials. V2 delivers a high specific capacity along with excellent rate capability and stability in successive electrochemical cycling. The theoretical calculations further confirm that V doping can enhance the electrical conductivity of materials, thus leading to superior rate capability.

ACKNOWLEDGEMENT

This research was funded by the Science and Technology Project of Guizhou Province [2018]1086.

References

1. X. Kong, Y. Zhang, S. Peng, J. Zeng, J. Zhang, *ACS Sustainable Chem*., 8 (2020) 1493.
2. S.P. Qiao, L.Z. Zhu, E.S. Han, L.N. Li, C.Y. Du, Y.Z. He, X. Yang, J.B. Liu, *Ionics*, 26 (2020) 5405.
3. G.H. Jiang, Y.N. Zhang, Q. Meng, Y.J. Zhang, P. Dong, M.Y. Zhang, X. Yang, *ACS Sustainable Chem. Eng.*, 44 (2020) 18138.
4. Z.Y. Chen, X.Y. Yan, M. Xu, K.F. Cao, H.L. Zhu, L.J. Li, J.F. Duan, *ACS Appl. Mater. Interfaces*, 9 (2017) 30617.
5. G. Wu, T.T. Jiang, X.H. Tian, T.B. Zhu, Y.K. Zhou, *Int. J. Electrochem. Sci.*, 13 (2018) 8006.
6. N.N. Zhao, Y.S. Li, X.X. Zhao, X.K. Zhi, G. Liang, *J. Alloys and Compounds*, 683 (2016) 123.
7. X.P. Huang, Y.C. Yao, F. Liang, Y.N. Dai, *J. Alloys and Compounds*, 743 (2018) 763.
8. Y.S. Meng, J. Xia, L. Wang, G.R. Wang, F.L. Zhu, Y. Zhang, *Electrochimica Acta*, 261 (2018) 96.
9. R. Martins, R. Gonçalves, C.M. Costa, S. Ferdov, S. Lanceros-Méndez, *Nano-Structures & Nano-Objects*, 11 (2017) 82.
10. W-C. Chien, K-N. Liu, S-C. Chang, C-C. Yang, *Thin Solid Films*, 660 (2018) 931.
11. X.F. Wang, Z.J. Feng, X.L. Hou, L.L. Liu, M. He, X.S. He, J.T. Huang, Z.H. Wen, *Chemical Engineering Journal*, 379 (2020) 122371.
12. B. Zhang, Y. Xu, J. Wang, J. Lin, C. Wang, Y. Chen, *Electrochimica Acta*, 322 (2019) 134686.
13. Z.Y. Chen, Q.F. Zhao, M. Xu, L.J. Li, J.F. Duan, H.L. Zhu, *Electrochimica Acta*, 186 (2015) 117.
14. S-Y. Chung, J.T. Bloking, Y-M. Chiang, *Nature materials*, 1 (2002) 123.
15. Z.R. Xu, L.B. Gao, Y.J. Liu, L. Li, *J. Electrochem. Soc.*, 163 (2016) A2610.
16. N.N. Zhao, Y.S. Li, X.K. Zhi, L. Wang, X.X. Zhao, Y.M. Wang, G.C. Liang, *J. Rare Earths*, 34 (2016) 180.
17. H-C. Liu, Y-M. Wang, C-C. Hsieh, *Ceramics International*, 43 (2017) 3201.
18. Y. Liu, Y. Gu, G. Luo, Z. Chen, F. Wu, X. Dai, Y. Mai, J. Li, *Ceramics International*, 46 (2020) 14863.
19. J. Xu, G. Chen, *Physica B*, 405 (2010) 803.
20. Z.Y. Chen, Z. Zhang, Q.F. Zhao, J.F. Duan, H.L. Zhu, *J. Nanosci. Nanotechnol.*, 19 (2019) 119.
21. D.X. Zhang, J. Wang, K.Z. Dong, A.M. Hao, *Computational Materials Science*, 155 (2018) 410.
22. I.D. Johnson, M. Lübke, O.Y. Wu, N.M. Makwana, G.J. Smales, H.U. Islam, RY. Dedigama, R.I. Gruar, C.J. Tighe, D.O. Scanlon, F. Corà, D.J.L. Brett, P.R. Shearing, J.A. Darr, *J. Power Sources*, 302 (2016) 410.
23. K.J. Kreder, A. Manthiram, *ACS Energy Lett.*, 2 (2017) 64.
24. S.S. Jiang, Y.S. Wang, *Solid State Ionics*, 335 (2019) 97.
25. C-Y Chiang, H-C. Su, P-J. Wu, H-J. Liu, C-W. Hu, N. Sharma, VK. Peterson, H-W. Hsieh, Y-F. Lin, W-C. Chou, C-H. Lee, J-F. Lee, aB-Y. Shew, *J. Phys. Chem. C*, 116 (2012) 24424.
26. N. Sofyan, D.Y. Putro, A. Zulfia, *International Journal of Technology*, 7 (2016) 1307.
27. F. Omenya, N.A. Chernova, Q. Wang, R.B. Zhang, M.S. Whittingham, *Chem. Mater.*, 25 (2013) 2691.
28. F. Omenya, N.A. Chernova, S. Upreti, P.Y. Zavalij, K-W. Nam, X-Q. Yang, MS. Whittingham, *Chem. Mater.*, 23 (2011) 4740
29. H.L. Zhang, Y. Gong, S. Yang, J. Li, J.Q. Li, Int. J. Electrochem. Sci., 13 (2018) 10427.
30. G.G. Xu, K.H. Zhong, J.M. Zhang, Z.G. Huang, *J. Appl. Phys,* 116 (2014) 063703.
31. J. Xu, G. Chen, *Physica B,* 405 (2010) 803.
32. G.G. Xu, K.H. Zhong, J.M. Zhang, Z.G. Huang, *Solid State Ionics,* 281 (2015) 1.
33. Y. Zhang, J.A. Alarco, J.Y. Nerkar, A.S. Best, G. A. Snook, P.C. Talbot, B.C.C. Cowie, *ACS Appl. Energy Mater.,* 3 (2020) 9158.
34. B. Xu, P. Dong, J.G. Duan, D. Wang, X.S. Huang, Y.J. Zhang, *Ceramics International,* 45 (2019) 11792.

35. P.P. Sun, H.Y. Zhang, K. Shen, Q. Fan, Q.Y. Xu, *J. Nanosci. Nanotechnol.*, 15 (2015) 2667.
36. Z.C. Shao, J.L. Xia, X.Q. Liu, G.Y. Li, *Materials and Manufacturing Processes*, 31 (2016) 695.
37. M. Chen, L-L. Shao, H-B. Yang, T-Z. Ren, G.H. Du, Z-Y. Yuan, *Electrochimica Acta*, 167 (2015) 278.
38. L-L. Zhang, G. Liang, A. Ignatov, M.C. Croft, X-Q. Xiong, I-M. Hung, Y-H. Huang, X-L. Hu, W-X. Zhang, Y-L. Peng, *J. Phys. Chem. C*, 115 (2011) 13520.
39. A. Moretti, G. Giuli, F. Nobili, A. Trapananti, G. Aquilanti, R. Tossici, R. Marassi, *J. Electrochem. Soc.*, 160 (2013) A940.